JOURNAL OF GEOPHYSICAL RESEARCH: SPACE PHYSICS, VOL. 118, 1–11, doi:10.1002/jgra.50172, 2013

Coincident particle and optical observations of nightside subauroral proton precipitation

Finn Søraas,[1,2] Karl M. Laundal,[1,2,3] and Maria Usanova[4]

Received 20 June 2012; revised 30 January 2013; accepted 31 January 2013.

[1] We report two instances of nightside subauroral proton precipitation observed during a geomagnetic storm: (1) An arc at $\approx 50^\circ$ magnetic latitude (MLAT), which extended roughly from midnight to 6 magnetic local time (MLT), and (2) A corotating spot at 51.5° MLAT, postmidnight. The proton precipitation was observed by both the IMAGE SI-12 proton aurora (Doppler-shifted Lyman-α) imager, and low-altitude Polar-orbiting Operational Environmental Satellites (POESs) that serendipitously traversed both the arc and the spot, providing in situ particle measurements. The Lyman-alpha emission and the particle observations match closely. The particle measurements showed that the energies of the precipitating protons extended to several hundred keV, but no enhancements in the protons below 20 keV were observed. Cluster observations showed that the ring current contained protons with energies extending from tens of eV to several hundred keV; thus, the particles are scattered into the atmosphere from an existing reservoir. Outside the luminous regions, but at the same magnetic latitude, the POES satellites observed localized regions with enhanced proton fluxes outside, but close to, the loss cone. This shows that the protons along a large region in MLT are subjected to pitch angle scattering. Model calculations of the plasmasphere show that the arc and the proton precipitation are located just inside the plasmapause. The intensity and longitudinal extension of the arc are modulated by the dynamical pressure in the solar wind. In the dusk sector, ground stations recorded electromagnetic ion cyclotron waves associated with localized proton precipitation just inside the plasmapause. This suggests that the proton precipitation is caused by wave/particle interaction.

Citation: Søraas, F., K. M. Laundal, and M. Usanova (2013), Coincident particle and optical observations of nightside subauroral proton precipitation, *J. Geophys. Res. Space Physics*, *118*, doi:10.1002/jgra.50172.

1. Introduction

[2] The main features of the aurora are the two auroral ovals found in each hemisphere. In addition to these ovals, one finds localized more distinct aurora beyond/outside and in the ovals itself. These features of the aurora have recently been reviewed by [*Frey*, 2007].

[3] Localized precipitation of energetic protons (LPEP) equatorward of the main auroral proton precipitation zone has been reported by *Søraas et al.* [1999]; *Frey et al.* [2004]; *Sandanger et al.* [2009]; *Yahnina et al.* [2002]. *Sandanger et al.* [2009] have shown that the enhanced proton precipitation occurs inside the plasmapause by comparing LPEP observations with near simultaneous determination of the plasmapause given by *Spasojevic et al.* [2003] and *Yahnina et al.* [2002] that LPEP also can occur in plasmaspheric plumes. *Sakaguchi et al.* [2007] report ground-based observation of isolated proton arcs, which appeared when intense geomagnetic Pc 1 pulsations were observed both in the premidnigh and postmidnight sector. The arc corresponds to a localized enhancement of the precipitating ions that was isolated equatorward from the main ion oval. *Sakaguchi et al.* [2008] have compared ground-based observations of subauroral proton aurora with particle measurements by Polar-orbiting Operational Environmental Satellites (POES) with precipitating protons in the (30 to 250) keV range. *Coumans et al.* [2002] compare SI12 observations in the auroral oval with model predictions of the interaction of auroral particles with the atmosphere based upon in situ proton and electron flux measured by POES spacecraft. They showed that in some regions, especially in the dusk sector, high-energy protons dominate the proton energy flux and account for a large fraction of Ly-α and other FUV emissions. *Yahnina et al.* [2002] have further shown that the proton precipitation at midlatitudes is connected with electromagnetic ion cyclotron (EMIC) wave generation, and suggested that they are the particle signature of EMIC generation. *Usanova*

[1] Department of Physics and Technology, University of Bergen, Bergen, Norway.
[2] Birkeland Centre for Space Science, Bergen, Norway.
[3] Teknova AS, Kristiansand, Norway.
[4] Department of Physics, University of Alberta, Edmonton, Canada.

Corresponding author: F. Søraas, Department of Physics and Technology, University of Bergen, Allegaten 55, 5007 Bergen, Norway. (finn.soraas@ift.uib.no)

2169-9380/13/10.1002/jgra.50172

et al. [2010] have shown that these enhancements, observed by a POES satellite, are directly connected with the occurrence of EMIC waves observed at ground and at a Cluster satellite that was conjugate to both the particle observations and the ground station.

[4] In the present paper, we will discuss subauroral phenomena connected to a proton arc and a spot observed during a geomagnetic storm on 10 and 11 November 2004. They resemble what has been referred to as nightside detached aurora (NDA) [*Zhang et al.*, 2005], and subauroral morning proton spots (SAMPS) [*Frey et al.*, 2004]. In both of the reported events, simultaneous in situ particle measurements from low Earth orbiting satellites (POES) and FUV images from the Imager for Magnetopause-to-Aurora Global Exploration (IMAGE) satellite are at hand. In addition, Cluster observations of ring current particles and ground-based observations of EMIC waves are used.

[5] In the following sections, we present the instrumentation related to the IMAGE and POES spacecrafts (Section 2) and the observations (Section 3). Sections 4 and 5 summarize and conclude the paper.

2. Instrumentation

[6] The IMAGE satellite [*Burch*, 2000] has an orbit with perigee around 1000 km and apogee at 7.2 Earth radii. The orbital period of the satellite is 14.2 h. The IMAGE SI-12 spectrographic imager views the Earth's upper atmosphere through a narrow passband centered at 121.8 nm, and blocks the emissions at 121.56 nm, from cold hydrogen. This means that SI-12 observes Doppler-shifted Ly-α emissions from descending hydrogen, produced as protons precipitate and charge exchange with the atmosphere. Its sensitivity peaks for 2 keV protons, but protons of higher energies can also be detected [*Frey et al.*, 2003]. However, as the proton energy increases, the Ly-α production becomes less efficient, and emissions are mostly produced at low altitudes, where it will be absorbed by O_2. *Coumans et al.* [2002] calculated that in the energy range of 30–80 keV, the efficiency expressed in counts pixel^{-1}s^{-1} per incident mW/m^2 will be 1.75, and in the energy range 80–240 keV, it will be 1.06. Above 240 keV, the efficiency will be negligible.

[7] The camera resolution is 128×128 pixels, the integration time is 5 s, and cadence is 123 s. On the 10 November event, the IMAGE satellite was at 2.5 – 5.5 R_E from the Earth. During the 11 November event, the altitude of the IMAGE satellite was only 2 – 3 R_E (relative to ground), and so SI-12 could resolve finer features in the ionosphere than usual (apogee observations).

[8] The orbits of the NOAA/POES satellites are polar and sun-synchronous at an altitude of about 850 km and with an orbital period of about 100 min. The orbits of the satellites cover different local times.

[9] The energetic protons are measured by two detectors, which are part of the Medium Energy Proton and Electron Detector (MEPED). The energy bands for the two detectors used in the present study are 30–80, 80–250, and 250–800 keV. One of the detectors is directed along the Earth-satellite radial vector. The atmospheric loss cone is about 60° at MLAT 50°. The pitch angle of the vertical detector is around 40° at this latitude thus well inside the loss cone and observes the precipitation flux that interacts with the atmosphere. The other MEPED detector looks normal to the first detector and observes slightly outside the loss cone. The proton detectors are sensitive to both protons and neutral particles, but give neither mass resolution nor the charge state of the particles. As MEPED does not distinguish between different ion species, the term protons are used throughout this paper (note that the SI-12 images only measures hydrogen emissions from precipitating protons). The electrons and protons with energies below 20 keV are measured by the Total Energy Detector (TED). TED measures at 0 and 30∘ with the vertical in four energy bands, 154 – 224, 688 – 1000, 2215 – 3075, and 6503 – 9457 eV, as well as the total energy in mW/m^2 for the energy range 150 eV to 20 keV. For a discussion of the MEPED instrument response to heavier ions, see *Søraas et al.* [2002]. A full description of the NOAA spacecraft and the MEPED instrument is given by *Evans and Greer* [2000]. *Yando et al.* [2011] have done a comprehensive Monte Carlo evaluation of the MEPED instrument, and they suggest a method for combining the electron and proton telescope data to obtain corrected fluxes for both species. This is useful because the MEPED electron and proton data can be hampered by cross talk under certain geomagnetic conditions.

3. Observations

[10] The storm started on 9 November 2004 and reached < –250 nT. A second main phase occurred the next day, with Sym-H reduction exceeding the first dip. The arc was observed on 10 November in the recovery phase of the first storm, between the two main phases. The spot was observed on 11 November, also during storm recovery. Note that this double-dip storm succeeded a stronger storm (< –350 nT) that started on 7 November (not shown), which had not fully recovered (Sym-H was < –50 nT at onset). The timeline of the storm and observations is shown in Figure 1.

3.1. The Proton Arc on 10 November

[11] The proton arc was observed by the IMAGE satellite at –50° magnetic latitude (MLAT), reaching from around midnight and into the morning sector. The arc was presented as the region entered the field of view, just after 00:00 UT, and faded away around 02:00 UT. Thus, the lifetime was at least 2 h.

[12] In Figure 2, an IMAGE SI-12 picture of the proton aurora in the Southern Hemisphere is shown. The proton arc extends from around 23 to 05 MLT, that is a length of 5000 km. The arc was also visible in the other IMAGE FUV cameras, Wideband Imaging Camera, and SI-13, which respond both to electron and proton precipitation. It was, however, relatively fainter in these images compared to the oval, indicating that the light was generated mainly by protons. This is supported by POES particle measurements. The arc is well separated from the main auroral zone that is located poleward of –56° MLAT. The light intensity varies along the arc. The black curve shows the footprint of the NOAA 16 satellite, which crossed the arc (moving poleward and towards the dusk) approximately at the time of the SI-12 exposure.

[13] Figure 3 shows the SI-12 intensity plotted along the NOAA 16 satellite track (top panel). For each NOAA measurement, the closest SI-12 pixel, in time and space,

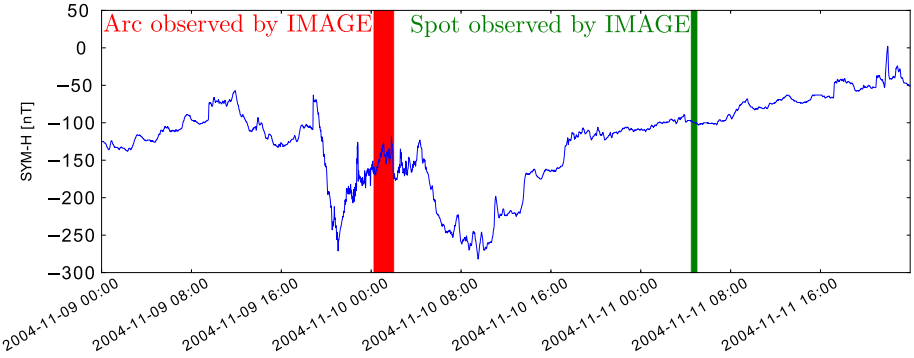

Figure 1. Sym-H from 9 November through 11 November 2004. The observation periods are indicated by red (arc) and green (spot).

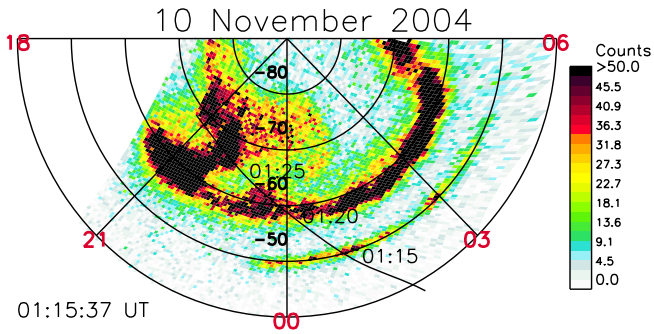

Figure 2. IMAGE SI-12 picture of the proton aurora in the Southern Hemisphere. The arc is seen to extend from premidnight to approximately 5 MLT. Also shown is the satellite track of NOAA 16. The satellite crossed the arc at 01:15 UT.

is used. The times of SI-12 exposures are shown as vertical dotted lines. Also shown (bottom panel) are the fluxes of precipitating protons, measured by NOAA 16, in three different energy bands, indicated by the colors. The solid curves show fluxes inside the loss cone, and the dashed curves show fluxes perpendicular to the field line (locally mirroring particles at the satellite altitude). There is very good correspondence between the optical arc (starting just after 01:15:30 UT) and the precipitating protons. In the arc, the proton intensity increases abruptly in the 30–80 and 80–250 keV bands. The fall in proton intensity is also very abrupt. Thus, the region of proton precipitation is very limited in latitude having a half width of 210 km at the satellite altitude. The arc seen by SI-12 is wider, which may be due to the point spread function of the instrument, or more likely by the precipitating protons spreading out in latitude, due to the multiple charge exchanges as they descend. The latter is also consistent with the calculated extension of the luminosity towards higher latitudes, since the field lines are tilted towards equator [*Synnes et al.*, 1998]. At around –56° MLAT, the equatorward boundary of the auroral oval is reached. The increase in the particles is more gradual here compared to the arc. The isotropic boundaries (IB) for the three energy channels are indicated by arrows. The IB for the highest energy band is at the lowest MLAT.

[14] In the Northern Hemisphere, NOAA 16 observed LPEP just before 00:49 UT (Figure 4). That is, in a region conjugate to the proton arc, thus, the subauroral proton precipitation is a conjugate phenomenon covering a large MLT region. There was no enhancement in the < 9.46 keV protons measured by the TED. Thus, there is no low energy proton precipitation in the arc.

[15] Figure 5 shows IMAGE SI-12 pictures from the start and at the end of the arc observation period. Also shown is an MLT keogram, derived from IMAGE SI-12 data, by integrating the intensity between –45° to –51° MLAT. This plot reveals the time development of the intensity and longitudinal extent of the arc during a 2-h period. The bottom panel shows a measure of the arc length (green), calculated as the number of bins (1/3 h wide) with more than nine counts/pixel, as well as the mean intensity of the arc (red) and the solar wind dynamic pressure (blue) measuremed by Geotail. The length of the arc could be determined from 00:50 UT (vertical dashed bar) when the whole arc is in the field of view of the SI-12 instrument. Geotail was located in the solar wind at 14, –17, and 7 R_E; thus, pressure changes affect the magnetosphere with very little time delay (a 3 min time shift has been applied). The dynamic pressure increased from ≈ 2 nPa to a peak of ≈ 25 nPa.

[16] Looking at the period after 00:50 UT, we notice that there seems to be a good correlation between the solar wind pressure and the arc extent and intensity. They both exhibit variations similar to the solar wind dynamic pressure. Particularly, the largest increase in pressure, seen at 01:45 UT, coincides with a brief, but strong increase in longitudinal extent and in the intensity. Smaller pressure variations also seem to correlate with arc intensity/length. Pressure pulses can increase the anisotropy of the particle distributions, generating EMIC waves [*Anderson and Hamilton*, 1993], which are suspected to cause the observed proton precipitation. *Laundal and Østgaard* [2008] have shown that the proton aurora is to a large extent modulated by the pressure, although that study was focused on the main oval. The good correlation seen in Figure 5 indicates that this is true also for subauroral proton precipitation.

[17] Another interesting feature seen just before 01:40 UT when the arc suddenly diminished and increased again in the next image. At the same time, there was a slight decrease in solar wind pressure. The intensity of the main

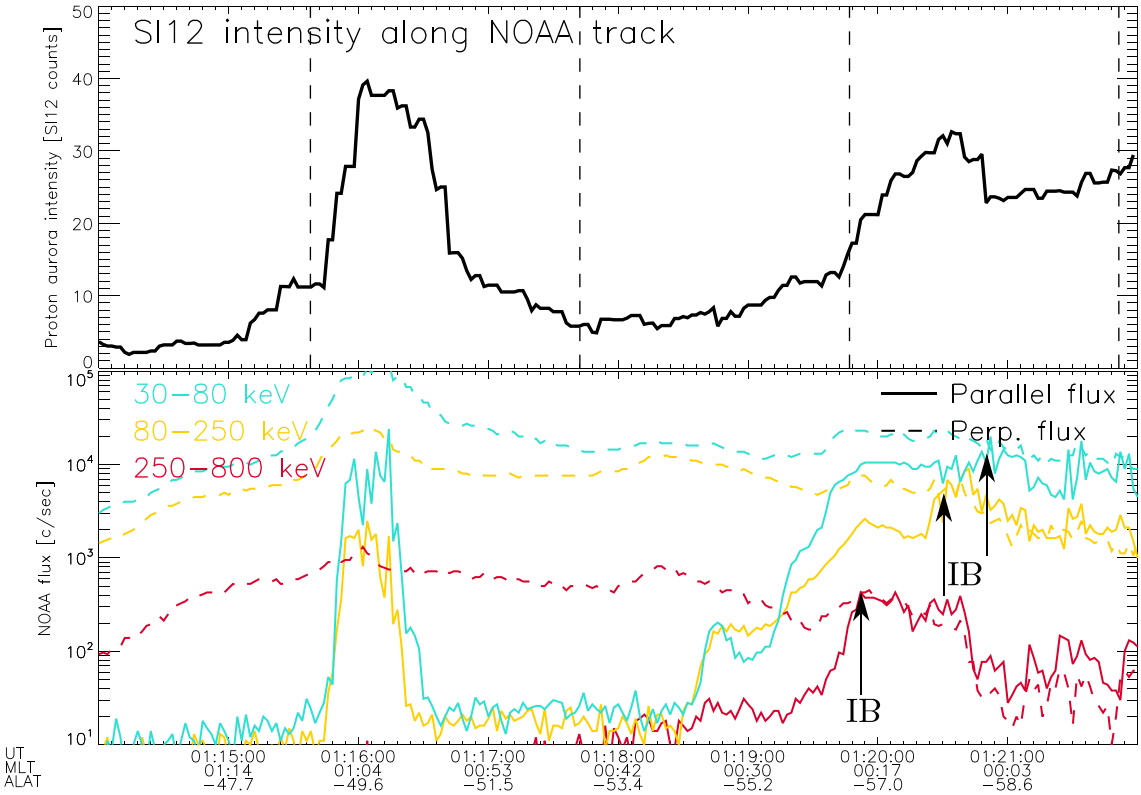

Figure 3. In situ particle measurements, and simultaneous SI-12 intensity along the satellite track. The top panel shows the intensity at the closest pixel from the satellite track (always less than 0.3° away), in the image taken closest in UT. The dotted vertical bars show the time of center of exposure in SI-12. The colored curves show precipitating particle flux in the channels indicated by the color. The arc is crossed just after 01:15, and the satellite enters the main oval at 01:19:15. The arrows indicate the isotropic boundary (IB) for the three energy channels.

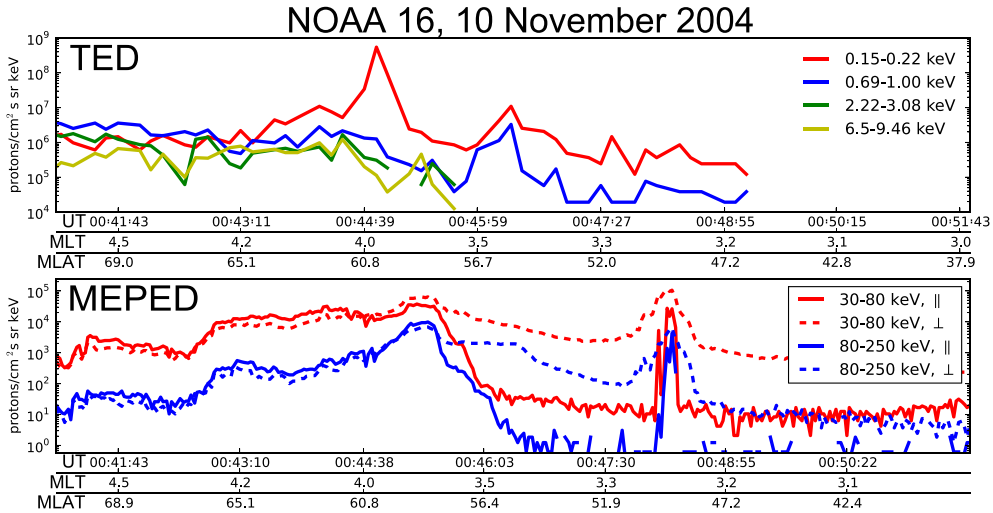

Figure 4. In situ particle measurements from both TED and MEPED detectors on NOAA 16, 10 November 2004. The figure shows that a spike is seen in the Northern Hemisphere in the postmidnight sector, showing the arc was a conjugate phenomenon. The flux of low energy particles (TED) shows no increase in this region.

oval in this image did not show a similar reduction, which suggests that the dropout is real and not due to a change in the SI-12 sensitivity.

3.2. The Spot Observations on 11 November 2004

[18] Figure 6 shows an IMAGE SI-12 picture of the Southern Hemisphere with a small auroral spot located

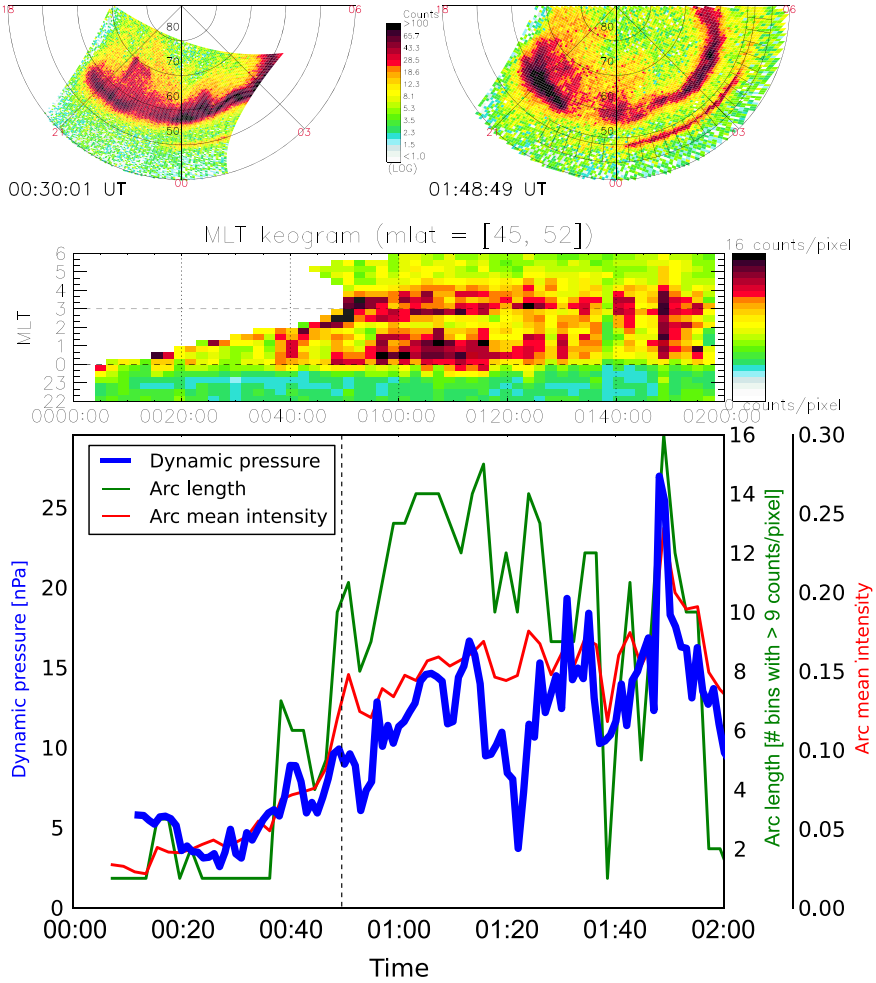

Figure 5. Time development of the arc luminosity: The upper pictures show two images with a visible arc, from the beginning and end of the observation period. The upper panel of the lower picture shows an MLT keogram, where each colored square reflects the average intensity in the boxes drawn in the upper right picture at various UTs. The bottom panel shows a measure of the longitudinal extent of the arc (green), mean arc intensity (red), and solar wind dynamic pressure measured by Geotail (blue).

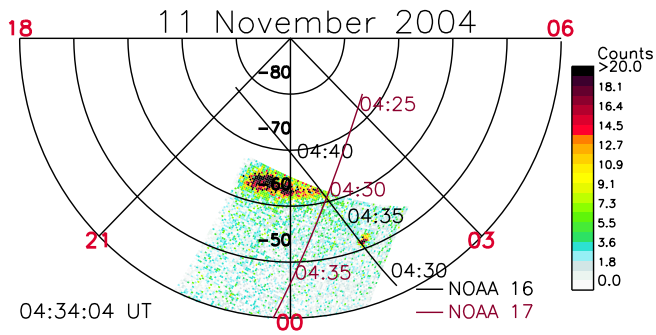

Figure 6. SI-12 image of the proton aurora, with a subauroral spot at 1:30 MLT. The satellite tracks of NOAA 16 and NOAA 17 are also shown. The NOAA 16 satellite traversed the spot approximately at the time of the picture. The NOAA 17 satellite track is well outside the spot.

at ≈ –51.5° MLAT (peak intensity) and at 01:30 MLT. The spot is well separated from the main auroral zone. The magnetic footprint of NOAA 16 and NOAA 17 are indicated, and fortuitously, NOAA 16 traversed the spot at 04:35 UT, almost at the same time as the IMAGE picture was taken. Thus, simultaneous observations of light and particles in a subauroral spot were obtained. NOAA 17 traversed the same MLAT as NOAA 16 but further towards midnight.

[19] The spot was visible from its entry in the field of view at 04:32 UT until it diminished at 05:03 UT (Figure 7).

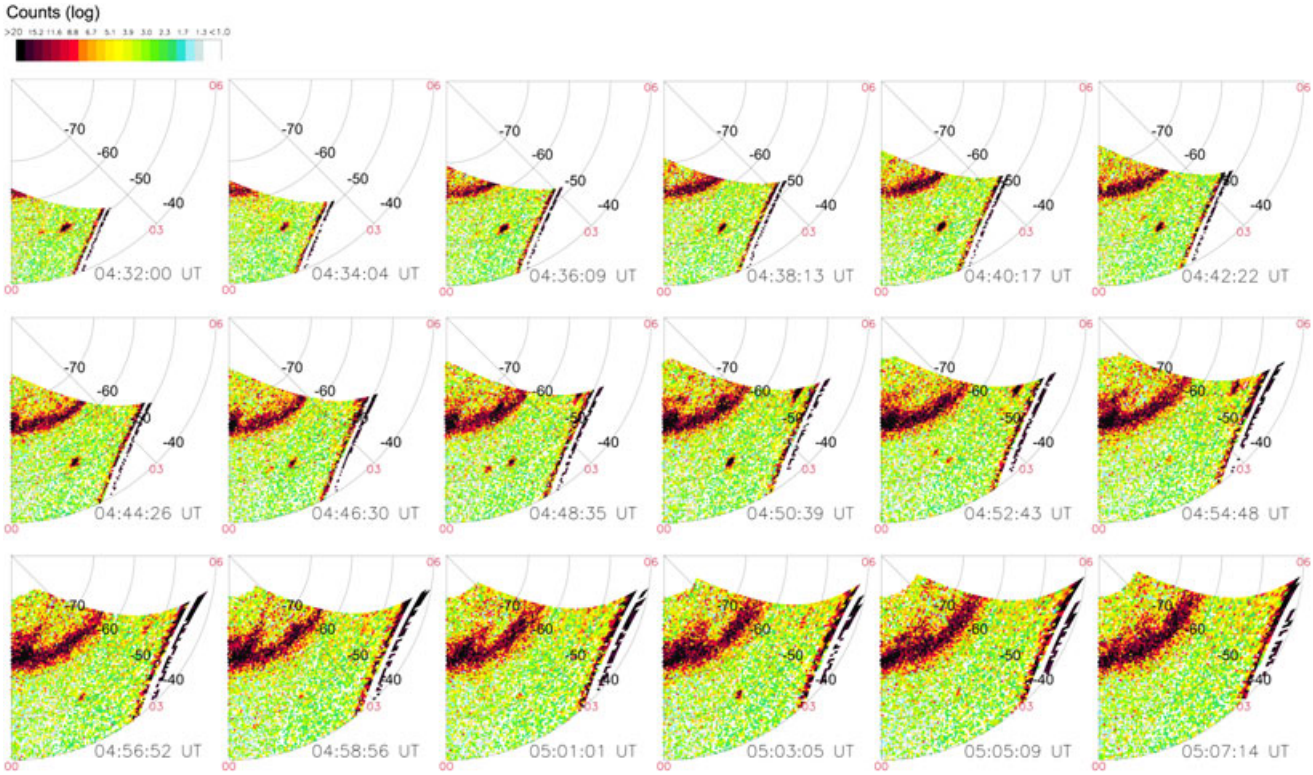

Figure 7. Series of SI-12 images, from the 00-03 MLT sector, spanning 04:32:00 (region entry to the field of view) to 05:07:14, when the spot had diminished.

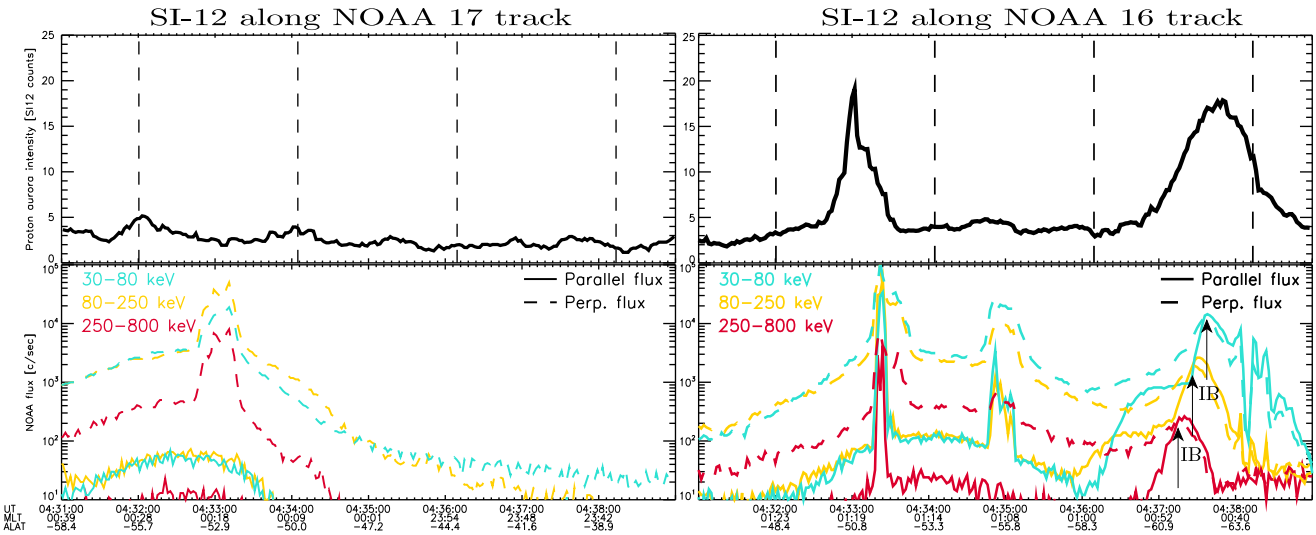

Figure 8. The top panels show SI-12 intensity along NOAA 17 (left column) and NOAA 16 (right column) satellite tracks. The bottom panels show perpendicular (dashed) and parallel (solid) proton flux, measured by NOAA 17 (left column) and 16 (right column). The colors indicate the energy bin. The data is from 11 November 2004.

Thus, its lifetime was at least 31 min. The location of the peak intensity moved monotonically from 01:32 to 01:50 MLT, while its geographic longitude fluctuated between 313° and 315°. The fixed position in geographic longitude (well within the expected variation from spot extent and satellite pointing inaccuracy) implies that the spot corotated with the Earth, with no discernible lag. The solar wind pressure was low (0.5 nPA) during the spot observations.

[20] The top panels in Figure 8 show the SI-12 intensity along the NOAA 17 (left column) and NOAA 16 (right column) tracks. The bottom panels show the particle flux measured by these satellites in the detectors pointing parallel

(solid) and perpendicular (dashed) to the field lines. In the right figure (along the NOAA 16 track), the proton spot is seen to nearly coincide with the precipitating protons. There is, however, a slight misalignment between the light and the particles. This could be due to the ∼ 1° inaccuracy in SI-12 pointing caused by the wobbling motion that affected the IMAGE satellite at the time of these images. In the region of the spot, the NOAA 16 proton intensity increased with nearly three orders of magnitude, and it is seen in all three channels 30–80, 80–250, and 250–800 keV in both the parallel and the perpendicular detectors.

[21] At –55° MLAT, another abrupt increase in the protons is seen. This increase is not matched by SI-12 measurements. This flux did not give a clear response in the SI-12 instrument, although a very small increase (∼ 1 count) may be seen in the SI-12 plot. The proton flux in the loss cone, however, is a factor of 10 lower than within the spot.

[22] NOAA 17 crossed the spot latitude approximately at the same time as NOAA 16, at 04:33 UT, but 1.5 h in MLT further towards midnight. At this time, NOAA 17 also observed a proton enhancement, but only in the locally mirroring protons (Figure 8, left column). No protons were measured in the parallel detector (inside the loss cone), and no increased luminosity was observed by SI-12.

[23] The particle observations show, however, that the proton scattering process takes place over a larger region in MLT than the light measurements indicate.

[24] In the region where the light is observed, the pitch angle scattering of the protons is strong, and the protons are driven into the loss cone. There is, however, a more extended region where the pitch angle scattering is weak and the protons outside the loss cone increase.

4. Discussion

[25] Both the arc and the spot are due to the precipitation of very energetic protons with energies above 30 keV and extending to several hundreds of keV. In the spot also, protons with energies above 250 keV were observed. No protons with energies below 20 keV were observed in the arc or the spot.

[26] In order to see if these particles arrive from the ring current, Cluster satellite observations were examined.

[27] Figure 9 shows Cluster observations from 10 November 2004. Cluster is moving towards perigee (L = 4.5) that is reached at 03:52 UT. In the bottom panel, ring current protons with energies up to hundreds keV are present. The precipitating protons are thus scattered from this population. Cluster also observes large fluxes of ions below 20 keV (top panel); but the POES observations show that if there is precipitation at this energy, the fluxes are too low to be detected. The middle panel shows the total magnetic field in the ring current.

[28] It is interesting to notice that in the LPEP, the three different particle energies have the same latitudinal extent; while in the auroral zone, the isotropic boundary (IB), marked with arrows in Figures 3 and 8, is found at lower latitudes for increasing energies. The protons at these auroral zone latitudes are believed to be chaotically scattered in the tail because their gyroradii are large in relation to the curvature of the tail magnetic field [*Sergeev et al.*, 1983]. Since the gyroradius increases with energy, the higher energy particles maintain an isotropic pitch angle distribution to lower latitudes. In the LPEP, however, a different scattering mechanism must be invoked. The most likely pro-

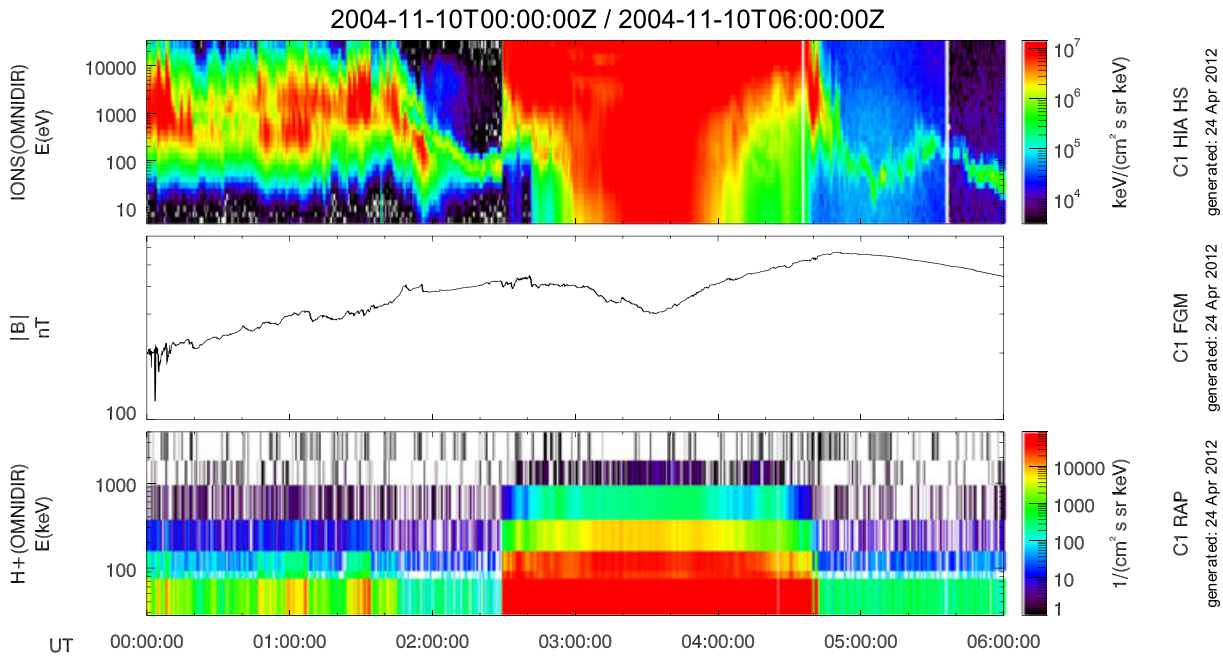

Figure 9. Cluster ion data on 10 November 2004 between 00 and 06 UT. The top panel show ions in the energy range 10 eV to 20 keV. The middle panel gives the strength of the magnetic field, and the bottom panel shows ions with energies from around 10 keV to 2 MeV. The position of Cluster at 03:42 UT is GSE 12820, –24158., and 45. km close to local time 8 and at 4.4 Earth radii.

cess would be wave/particle scattering that is independent of the field line curvature.

4.1. EMIC Waves

[29] Observations of ion cyclotron waves in the inner magnetosphere indicate that these waves exist over limited spatial regions that varies with time and that their occurrence frequency increases with L and occur mainly in the afternoon sector [*Anderson et al.*, 1992]. Studies with Viking [*Erlandson et al.*, 1990] found Pc 1 waves at the plasmapause, but also that Pc 1 wave events were not associated with gradients in the plasma density and occurred at latitudes above the expected position of the plasmapause. *Thorne and Horne* [1992] examined the propagation and amplification of ion cyclotron waves, and they found that the plasmapause density gradient plays an important role in the gain of these waves. The energetic ring current ions are the source of free-energy used in the wave amplification.

[30] Early theoretical studies have shown that the EMIC wave growth leads to the isotropization of the initially unstable proton distribution and consequent pitch angle scattering and loss of particles into the ionosphere (e.g. *Cornwall* [1965]). The resonant energies for ion interaction with EMIC waves depend upon the magnetic energy per particle $E_m = B^2/8\pi N$ [*Kennel and Petschek*, 1966], where B is the magnetic field and N is the plasma density. EMIC wave growth results only if the pitch angle anisotropy of the protons exceeds a critical value A_c [*Kennel and Petschek*, 1966]. The relation between the energy of the resonant proton, E_r and E_m is $E_r = E_m/\left(A_c^2(1+A_c)\right)$. This is simply the statement that the protons must have enough energy, E_r, to satisfy the Doppler-shifted cyclotron resonance condition in order to resonate with the waves. *Cornwall et al.* [1971] noted that this condition took place just within the plasmapause so that maximum instability of EMIC waves should occur in this region.

[31] Due to the lack of direct observations of the plasmapause/plasmasphere during our events, a three-dimensional dynamic model of the plasmasphere developed by *Pierrard and Stegen* [2008] has been used.

[32] In the top panel of Figure 10, the modeled plasma density in the equatorial plane at MLT 02 pertinent to the POES 16 LPEP and the IMAGE arc observations is shown. The position of the arc is indicated, and it appears just inside the plasmapause at $L = 2.51$. In the bottom panel, the energies E_m and E_r are shown. E_r is calculated for an anisotropy value $A_c = 0.5$. At the plasmapause, there is a large drop in the minimum resonant energy E_r from a few hundred keV and down to around 20 keV. This means that protons with energies above 20 keV can resonate with the EMIC waves and be scattered into the loss cone, and protons with energies below will not interact with the waves. Both of these claims are in accordance with the observations, the high energy protons precipitate, and the low energy protons do not appear in the loss cone. This is, however, only an illustrative example where $A_c = 0.5$ is within the range of values given by *Cornwall* [1965] for the anisotropy and the plasma density is taken from a model.

[33] We do not have observations of EMIC waves in either hemisphere in the MLT sector of the arc. In the Northern Hemisphere, however, the Lucky Lake (MLAT = 60, MLONG = 314.2), Parksite (MLAT = 61.1, MLONG = 313.7), and Gakona (MLAT= 63.1, MLONG= 266.8) stations all showed intense EMIC waves at around 0.3 Hz between 23:40 UT on 9 November to 02 UT on 10 November covering the time of the arc observation. The pul-

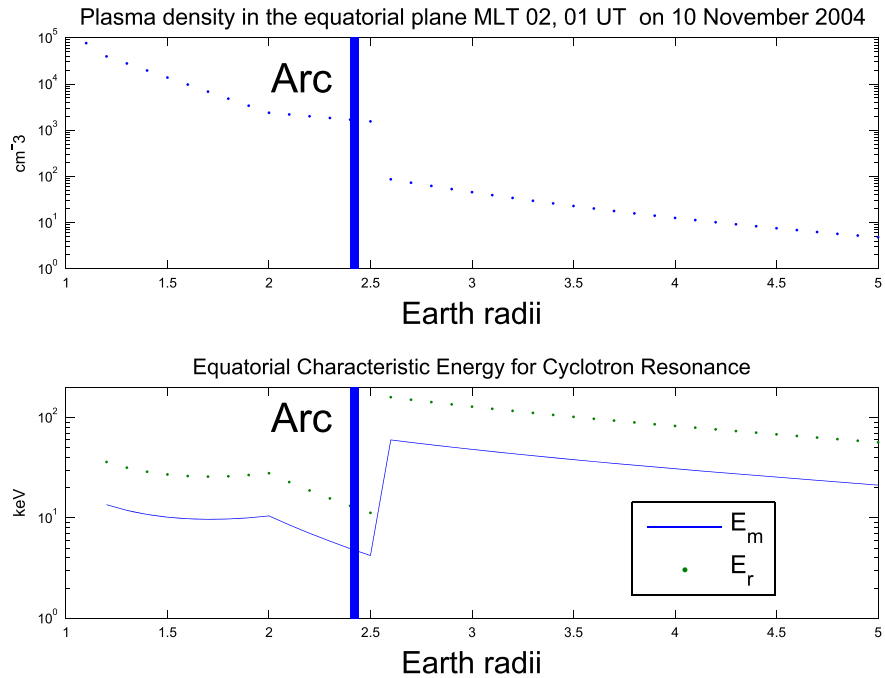

Figure 10. The top panel shows model calculations of the plasma density in the equatorial plane on 10 November 01 UT. The bottom panel gives the critical and the minimum resonance energies. In both panels, the values are along the radial distance at MLT 02.

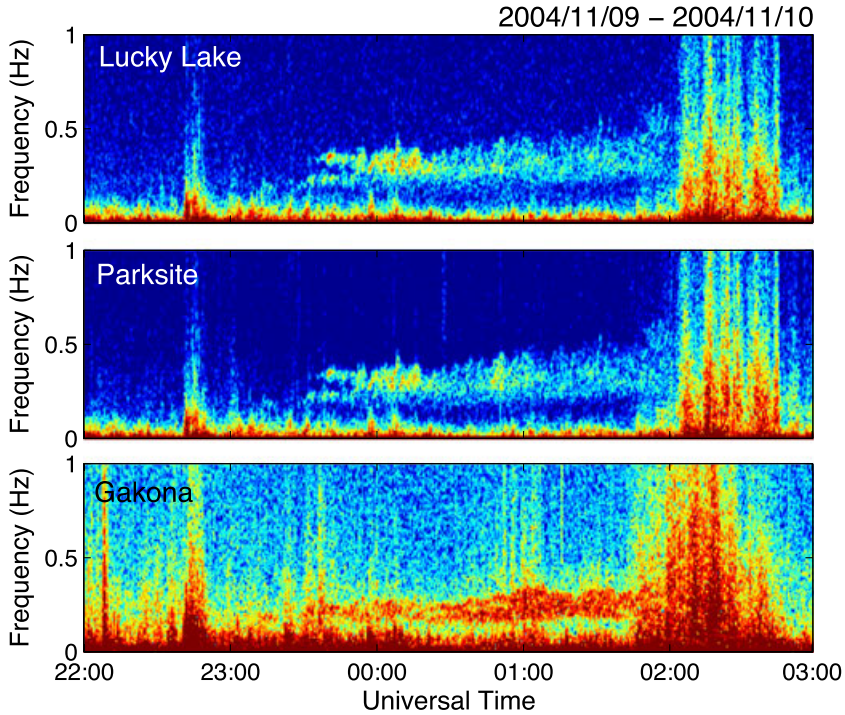

Figure 11. Spectrograms of the D-component (magnetic East-West) of magnetic field from the Lucky Lake (L = 3.94), Parksite (L = 4.23), and Gakona (L = 4.9) stations between 22 and 03 UT on 9–10 November 2004. During the arc observations, the ground magnetometer stations are located in the dusk sector.

sation data from the three stations are shown in Figure 11. The EMIC emissions spanned the range of magnetic local times between MLT 15:50 and 18:30 (at Lucky Lake and Parksite) and MLT 12:10–15 (at Gakona).

[34] Duskside EMIC waves were often observed by the CRRES satellite mission in association with enhanced cold plasma densities (*Fraser and Nguyen* [2001]) suggestive detached plumes or duskside plasmaspause bulge might be one of the source locations for EMIC waves. Further CRRES studies (see *Fraser et al.* [2010] and *Halford et al.* [2010]) showed that EMIC waves were frequently observed during the recovery phase of magnetic storms that is also consistent with our observations in the afternoon/dusk sector. We can, however, not conclude that the protons in the arc are scattered by EMIC waves, as we have no observations of EMIC waves in this MLT sector. Furthermore, many studies (*Anderson et al.* [1992]; *Fraser and Nguyen* [2001]) have shown that the occurrence rate of EMIC waves in the postmidnight local times are extremely low. The protons in the arc could thus be subjected to some other scattering mechanism than EMIC waves. This does not, however, rule out that the protons in the arc could be associated with EMIC waves but does suggest that it is likely to be an infrequent occurrence.

[35] Figure 12 shows proton data in two energy bands, 30–80 and 80–250 keV, for both precipitating and locally mirroring protons observed by POES 15. The satellite encounters LPEP at MLAT = 55 and MLT = 17 : 36 that is in the same MLT sector as the Lucky Lake and Parksite stations and about 5° south of them. The *Pierrard and Stegen* [2008] model predicted the plasmapause to be at 54 MLAT that is close to the observed LPEP. These observations around dusk are away from the arc, but they support an association between EMIC, LPEP, and the plasmapause position in accordance with earlier observations *Sandanger et al.* [2009] and *Yahnina et al.* [2002].

[36] *Frey* [2007] describes and classifies different types of aurorae beyond the main oval. Among the categories that he describes, the ones that are most similar to our observations are nightside detached auroras (NDA), and (in the case of the spot) subauroral morning proton spots (SAMPS). However, there are some important differences that we discuss below.

[37] The arc is most similar to NDAs that were studied extensively by *Zhang et al.* [2005]. The most important similarity is that NDAs are seen as subauroral proton precipitation on the nightside (although less frequently postmidnight), during storm recovery. Their latitudes are well predicted by the associated value of *Dst*, which in the case of the arc would be –52.5° (*Dst* = –150 nT), slightly poleward of the observed location. The energy of the protons was reported by *Zhang et al.* [2005] to be in the order of 10 keV, and possibly higher. Since they used Defense Meteorological Satellite Program (DMSP), energies higher than 30 keV could not be detected. Thus, if the arc is indeed an NDA, our observations show that such aurorae can be associated with energies in the 100 keV range, but in this case, less than 250 keV. An important difference between NDAs and the arc is the longitudinal extent, which seems to be larger in the present observations.

[38] The spot shares many of the above characteristics and may thus also be a similar phenomenon as the NDAs reported by *Zhang et al.* [2005]. However, the observed spot also shares some characteristics with subauroral morn-

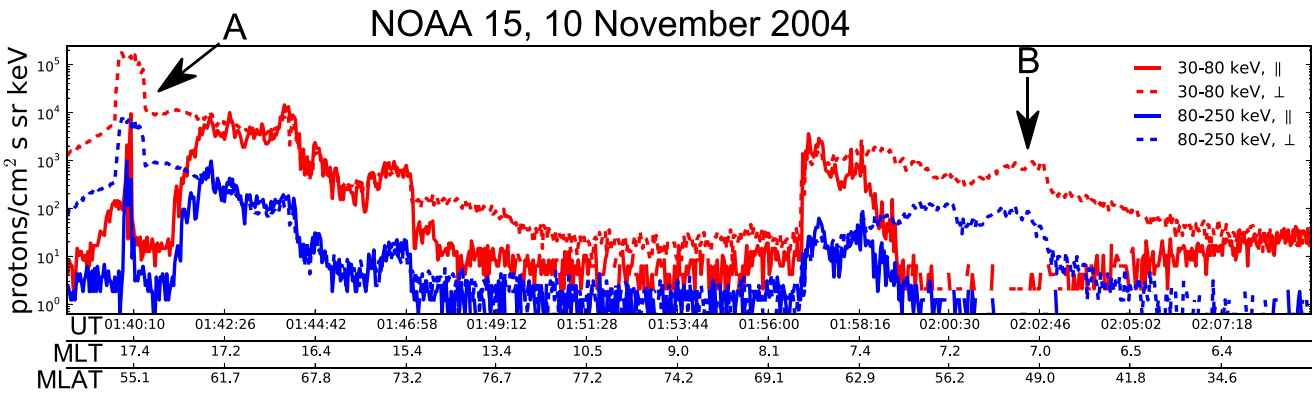

Figure 12. MEPED particle measurements from NOAA 15. The satellite passed close to the Lucky Lake and Parksite stations when it observed a spike (arrow labeled A). The arrow labeled B indicates a region at dawn with an increase in weak scattering (outside the loss cone), which may be a continuation of the arc observed at earlier hours.

ing proton spots (SAMPS) [*Frey et al.*, 2004]. These spots are reported to be caused by high energy proton precipitation, although the extent of the energy is not known; since this study also only reported DMSP measurements. SAMPS also corotate, are stable and occur during storm recovery—all traits shared by our observations. *Frey et al.* [2004] also reported a very good linear relationship between minimum *Dst* and the spot latitude. The latitude of the spot reported in the present paper is 1.5° equatorward from the [*Frey et al.*, 2004] regression line (their Figure 7). The one important difference between our observation and SAMPS is the magnetic local time. The earliest local time reported by *Frey et al.* [2004] was 4.5, while our spot is seen as early as 1.4. If this spot is indeed the same phenomenon as SAMPS, then the particle measurements reported here show that the proton energies are higher than 250 keV, and possibly as high as 800 keV. Measurements from the energy channel 800–2500 keV (not shown) show that there was a small increase in the flux of locally mirroring particles, but no enhancement in the loss cone.

5. Summary and Conclusions

[39] We have reported observations of two types of subauroral proton aurora, seen by the IMAGE SI-12 camera, with simultaneous in situ particle measurements by NOAA POES satellites. Both observations were done during the same geomagnetic storm but one day apart. The observations can be summarized as follows: (1) An arc at –50° magnetic latitude, primarily located in the midnight-dawn sector, associated with precipitating protons with energies reaching at least 80 keV, but not higher than 250 keV; (2) A corotating spot at ≈ –51° magnetic latitude, associated with precipitating protons with energies above 250 keV, but not higher than 800 keV. In both cases, no protons with energies below 20 keV were observed.

[40] There is an overall good correspondence between the light emissions and the particles, although the Lyman-alpha emission is somewhat broader. The particle observations reveal, however, the true dimensions of the precipitation region at the satellite altitude that amounts to 210 km for the proton arc. One should also note that the region of precipitation is the same for all energies in contrast to in the main oval where the location of the isotropic boundary (IB) depends on energy. Observations of ring current particles show that these protons could be scattered into the loss cone from this reservoir and not subjected to local accelerations. The intensity and extension in MLT of the arc is modulated by the solar wind pressure.

[41] The measurements further show that the pitch angle scattering occurs in a wider MLT-region than given by the Lyman-alpha emissions. This suggests that the scattering process has a larger longitudinal extent than indicated by the luminosity. The light observations give only information on where the scattering process is intense, and the protons are brought into the loss cone. The light indicates where there are sufficient particles within the loss cone to give detectable light emissions. The particle measurements, however, reveal the whole region of particle scattering both where the scattering is sufficient to bring particles into the loss cone and where only the locally mirroring particles are increased. Observations show that the LPEP is a conjugate phenomena occurring at the same MLT and MLAT in the two hemispheres.

[42] Comparing the LPEP observations with model predictions of the plasmapause reveal that they occur just within the plasmapause. This is in accordance with direct observations of LPEP and the plasmapause position [*Sandanger et al.*, 2009]. The model thus gives a fairly accurate position of the plasmapause. EMIC waves are observed in the dusk sector coincident with LPEP at the plasmapause in accordance with the prediction [*Cornwall et al.*, 1971] that the proton distribution is unstable and will generate EMIC waves. Our findings thus support many studies mentioned in Section 1 that show a close correspondence between LPEP and EMIC waves.

[43] The arc and spot resemble previous observations of nightside detached auroras [*Zhang et al.*, 2005] and, in the case of the spot, subauroral morning proton spots [*Frey et al.*, 2004]. Similarly to SAMPS and NDAs, the most likely mechanism for scattering the protons into the loss cone is an interaction between particles and waves at the plasmapause. This conclusion is further supported by the absence of low energy protons, as the energy of the particles must exceed a critical value before it can take part in interaction with waves.

[44] **Acknowledgments.** We acknowledge Viviane Pierrard, Belgian Institute for Space Aeronomy for providing model calculation of the plasma-sphere on 10 November 2004, and Kanji Hayashi at Department of Earth and Planetary Physics, The University of Tokyo for the Lucky Lake, Parksite, and Gakona observations. We thank CAA for the Cluster data and Space Weather Prediction Center, NOAA for maintaining the POES program. Thanks to the referees for valuable comments and suggestions.

References

Anderson, B. J., and D. C. Hamilton (1993), Electromagnetic ion cyclotron waves stimulated by modest magnetospheric compressions, *J. Geophys. Res.*, *98*, 11,369–11,382.

Anderson, B. J., R. E. Erlandson, and L. J. Zanetti (1992), A statistical study of pc 1-2 magnetic pulsations in the equatorial magnetosphere, 1. Equatorial occurrence distributions, *J. Geophys. Res.*, *92*, 3075–3088, doi:10.1029/91JA02706.

Burch, J. L. (2000), IMAGE mission overview, *Space Sci. Rev.*, *91*, 1–14.

Cornwall, J. M. (1965), Cyclotron instabilites and electromagnetic emissions in the ultra low frequency and very low frequency ranges, *J. Geophys. Res.*, *70*, 64–69, doi:10.1029/JZ070i001p00061.

Cornwall, J. M., F. V. Coroniti, and R. M. Thorne (1971), Unified theory of SAR arc formation at the plasmapause, *J. Geophys. Res.*, 4428–4445, doi:10.1029/JA076i019p04428.

Coumans, V., J.-C. Gérard, B. Hubert, and D. S. Evans (2002), Electron and proton excitation of the FUV aurora: Simultaneous IMAGE and NOAA observations, *J. Geophys. Res.*, *107*(A11), doi:10.1029/2001JA009233.

Erlandson, R. E., L. J. Zanetti, T. A. Potemra, L. P. Block, and G. Holmgren (1990), Viking magnetic and electric field observations of pc 1 waves at high latitudes, *J. Geophys. Res.*, *95*, 5941–5955, doi: 10.1029/JA095iA05p05941.

Evans, D. E., and M. S. Greer, (2000), Polar orbiting environmental satellite space environment monitor, 2, Instrument descriptions and archive data documentation, *Tech. Rep.*, Natl. Oceanic and Atmos. Admin., Boulder, Colo.

Fraser, B. J., and T. S. Nguyen (2001), Is the plasmapause a preferred source region of electromagnetic cyclotron waves in the magnetosphere?, *J. Atmos. Solar-Terr. Phys.*, 1225–1247.

Fraser, B. J., R. S. Grew, S. K. Morley, J. C. Green, H. J. Singer, T. M. Lotoaniu, and M. F. Thomsen (2010), Storm time observations of electromagnetic ion cyclotron waves at geosynchronous orbit: Goes results, *J. Geophys. Res.*, *115*, 5208, doi:10.1029/2009JA014516 .

Frey, H. U. (2007), Localized aurora beyond the auroral oval, *Reviews of Geophysics*, *45*, 1003, doi:10.1029/2005RG000174.

Frey, H. U., S. B. Mende, T. J. Immel, J.-C. Gerard, B. Hubert, S. Habraken, J. Spann, G. R. Gladstone, D. V. Bisikalo, and V. I. Shemantovich (2003), Summary of quantitative interpretation of IMAGE far ultraviolet auroral data, *Space Sci. Rev.*, *109*, 255–283 , doi:10.1023/B:SPAC.0000007521.

Frey, H. U., G. Haerendel, S. B. Mende, W. T. Forrester, T. J. Immel, and N. Ostgaard (2004), Subauroral morning proton spots SAMPS as a result of plasmapause-ring current interaction, *J. Geophys. Res.*, *109*, 10305, doi:10.1029/2004JA010516.

Halford, A. J., B. J. Fraser, and S. K. Morley (2010), EMIC wave activity during geomagnetic storm and nonstorm periods: CRRES results, *J. Geophys. Res.*, *115*, 12248, doi:10.1029/2010JA015716.

Kennel, C. F., and H. E. Petschek (1966), Limit on stably trapped particle fluxes, *J. Geophys. Res.*, *71*, 1–28, doi:10.1029/JZ071i001p00001.

Laundal, K. M., and N. Østgaard (2008), Persistent global proton aurora caused by high solar wind dynamic pressure, *J. Geophys. Res.*, *113*, 8331, doi:10.1029/2008JA013147.

Pierrard, V., and K. Stegen (2008), A three-dimensional dynamic kinetic model of the plasmasphere, *J. Geophys. Res.*, *113*, 10209, doi:10.1029/2008JA013060.

Sakaguchi, K., K. Shiokawa, A. Ieda, Y. Miyoshi, Y. Otsuka, T. Ogawa, M. Connors, E. F. Donovan, and F. J. Rich (2007), Simultaneous ground and satellite observations of an isolated proton arc at subauroral latitudes, *J. Geophys. Res.*, *112*, 4202, doi:10.1029/2006JA012135.

Sakaguchi, K., K. Shiokawa, Y. Miyoshi, Y. Otsuka, T. Ogawa, K. Asamura, and M. Connors (2008), Simultaneous appearance of isolated auroral arcs and Pc 1 geomagnetic pulsations at subauroral latitudes, *J. Geophys. Res.*, *113*, 5201, doi:10.1029/2007JA012888.

Sandanger, M., F. Søraas, M. Sørbø, K. Aaarsnes, K. Oksavik, and D. S. Evans (2009), Relativistic electron losses related to EMIC waves during CIR and CME storms, *J. Atmos. Solar-Terr. Phys.*, *71*, 1126–1144, doi:10.1016/j.jastp.2008.07.006.

Sergeev, V. A., E. M. Sazhina, N. A. Tsyganenko, J. Å. Lundblad, and F. Søraas (1983), Pitch-angle scattering of energetic protons in the magnetotail current sheet as the dominant source of their isotropic precipitation into the nightside ionosphere, *Planet. Space Sci.*, *31*, 1147–1155.

Søraas, F., K. Aarsnes, J. Å. Lundblad, and D. S. Evans (1999), Enhanced pitch angle scattering of protons at mid-latitudes during geomagenic storms, *Phys. Chaem Earth (C)*, *24*, 287–292.

Søraas, F., K. Aarsnes, K. Oksavik, and D. S. Evans (2002), Ring current intensity estimated from low-altitude proton observations, *J. Geophys. Res.*, *107*(A7), doi:10.1029/2001JA000123.

Spasojevic, M., J. Goldstein, D. L. Carpenter, U. S. Inan, B. R. Sandel, M. B. Moldwin, and B. W. Reinisch (2003), Global response of the plasmasphere to a geomagnetic disturbance, *J. Geophys. Res.*, *108*(A9), doi: 10.1029/2003JA009987.

Synnes, S. A., F. Søraas, and J. P. Hansen (1998), Monte-Carlo simulation of proton aurora, *J. Atmos. Solar-Terr. Phys.*, *60*, 1695–1705.

Thorne, R. M., and R. B. Horne (1992), The contribution of ion-cyclotron waves to electron heating and SAR-arc excitation near the storm-time plasmapause, *Geophys. Res. Lett.*, *19*, 417, doi:10.1029/92GL00089.

Usanova, M. E., et al. (2010), Conjugate ground and multisatellite observations of compression-related EMIC Pc1 waves and associated proton precipitation, *J. Geophys. Res.*, *115*, 7208, doi:10.1029/2009JA014935.

Yahnina, T. A., A. G. Yahnin, J. Kangas, and J. Manninen (2002), Localized enhancements of energetic proton fluxes at low altitudes in the subauroral region and their relation to Pc1 pulsations, *Cosmic Research*, *40*, 213–223, doi:10.1023/A:1015968702640.

Yando, K., R. M. Millan, J. C. Green, and D. S. Evans (2011), A Monte Carlo simulation of the NOAA POES medium energy proton and electron detector instrument, *J. Geophys. Res.*, *116*, 10231, doi:10.1029/2011JA016671.

Zhang, Y., L. Paxton, D. Morrison, B. Wolven, H. Kil, and S. Wing (2005), Nightside detached auroras due to precipitating protons/ions during intense magnetic storms, *J. Geophys. Res.*, *110*, 2206, doi: 10.1029/2004JA010498.